

PAPER

Analysis of current crowding in thin film contacts from exact field solution

To cite this article: Peng Zhang *et al* 2015 *J. Phys. D: Appl. Phys.* **48** 475501

View the [article online](#) for updates and enhancements.

Related content

- [Current flow in a 3-terminal thin film contact with dissimilar materials and general geometric aspect ratios](#)
Peng Zhang, Derek M H Hung and Y Y Lau
- [A more reliable measurement method for metal/graphene contact resistance](#)
Shaoqing Wang, Dacheng Mao, Zhi Jin *et al.*
- [Design considerations for AlGaIn-based UV LEDs emitting near 235 nm with uniform emission pattern](#)
Mickael Lapeyrade, Johannes Glaab, Arne Knauer *et al.*

Recent citations

- [Laser Processing Methods for Perovskite Solar Cells and Modules](#)
Keith G. Brooks and Mohammad Khaja Nazeeruddin
- [Interface Engineering of Electrical Contacts](#)
Sneha Banerjee *et al*
- [Space-charge limited current in nanodiodes: Ballistic, collisional, and dynamical effects](#)
Peng Zhang *et al*



IOP | ebooks™

Bringing together innovative digital publishing with leading authors from the global scientific community.

Start exploring the collection—download the first chapter of every title for free.

Analysis of current crowding in thin film contacts from exact field solution

Peng Zhang, Y Y Lau and R M Gilgenbach

Department of Nuclear Engineering and Radiological Sciences, University of Michigan, Ann Arbor, MI 48109-2104, USA

E-mail: umpeng@umich.edu

Received 5 July 2015, revised 31 August 2015

Accepted for publication 7 September 2015

Published 22 October 2015



CrossMark

Abstract

The paper presents a systematic evaluation of current crowding and spreading resistance in thin film contacts, based on the exact field solution that contains very large contrasts in dimensions and resistivity. It is found that current crowding becomes more severe as the interface specific contact resistivity decreases, the resistivity ratio of the contact electrode to the thin film decreases, or the thickness of either the contact or the thin film decreases. The current transfer length L_T from our exact field solution is compared to that of transmission line model (TLM), $L_{TLM} = (\rho_c/\rho_{sh})^{1/2}$, where ρ_c is the interface specific contact resistivity, and ρ_{sh} is the sheet resistance of the thin film under contact. It is found that, if ρ_c is small, L_T is bounded by the smaller of the two dimensions—thin film thickness and contact size. As ρ_c increases, L_T increases, but saturates at a constant value, determined by the smaller of the two dimensions—contact size and L_{TLM} . The total contact resistance is decomposed into three components: the interface resistance due to ρ_c , the spreading resistance due to current crowding, and the resistance due to the contact electrode. Unambiguously identified, each component is explicitly evaluated and compared in detail.

Keywords: electrical contact, current crowding, specific contact resistance, spreading resistance, joule heating

(Some figures may appear in colour only in the online journal)

1. Introduction

Current crowding and contact resistance are becoming increasingly important in the miniaturization of electronics [1–5]. How to accurately characterize these effects is an important issue [6–10]. Over a large range of resistivity and dimensions in the contact, they are very difficult to obtain accurately from finite element method (FEM), especially when there are mathematically sharp corners. Here, we evaluate them systematically, using the exact field solution we recently constructed [7]. The calculated current transfer length is compared with that of the transmission line model (TLM [6]). The well-known TLM approach [6,9] gives the contact resistance as $R_c^{TLM}W = \sqrt{\rho_c\rho_{sh}} \coth(a/L_{TLM})$, where $L_{TLM} = \sqrt{\rho_c/\rho_{sh}}$ is the transfer length, defined as the length scale over which most of the current from a contact to thin film flows, and W denotes the width in the dimension

perpendicular to the paper. From this expression, the TLM approach is not applicable in the limit of $\rho_c \rightarrow 0$, where both R_c^{TLM} and L_{TLM} approach zero [6,9]. TLM omits the fringing field near the contact edge, thus it is unable to account for the effects of current crowding and constriction (spreading) resistance. TLM also ignores the effects of electrode properties ρ_1 , h_1 (figure 1). Our exact solution provides a much more detailed evaluation of the contact resistance and current crowding. The contributions to the total contact resistance from the individual components of the contacts are unambiguously identified, evaluated, and compared.

2. Model description

Consider a pair of identical contacts formed on top of a conducting layer, which is laid on an insulating substrate, as shown in figure 1. The dimensions (h_1 , h_2 , a , L) and electrical

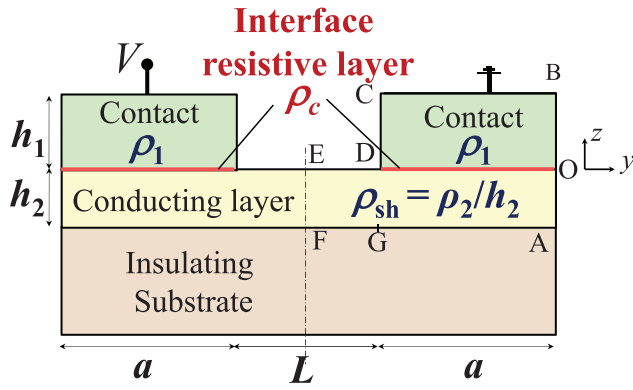


Figure 1. Electrical contact model. An infinitesimally thin resistive interface layer is sandwiched between the conducting layer and the contact. The structure is symmetric about the axis along EF. Note that ρ_1 and ρ_2 have units in $\Omega \text{ m}$, $\rho_{\text{sh}} = \rho_2/h_2$ is in Ω/\square , and ρ_c is in $\Omega \text{ m}^2$.

resistivity (ρ_1, ρ_{sh}) of the contacts and the conducting layer are specified in figure 1. An infinitesimally thin interface layer, of specific interfacial resistivity ρ_c (also termed specific contact resistivity), is sandwiched between both the contacts and the conducting layer. Current flows from one contact to the other through the conducting layer, when a bias voltage is applied between them. The potential distribution in figure 1 is very difficult to solve accurately by FEM based codes, especially if there is a large contrast among the geometric ratios or resistivity ratios. We have recently developed the exact field solution for the potential profile Φ for arbitrary values of dimensions h_1, h_2, a, L , and resistivities ρ_1, ρ_{sh} , and ρ_c by Fourier series expansion [7]. Due to symmetry, we need only to consider (the right) half of the geometry in figure 1. The Laplace equation and boundary conditions are summarized in table 1. The exact solution for $\Phi_{\text{II}}(y, z)$ within OEFA is given in [7]. The exact solution for $\Phi_{\text{I}}(y, z)$ within OBCD is recorded as $\Phi_{\text{I}}(y, z) = A_0(z - h_1) + \sum_{n=1}^{\infty} A_n \cos(k_n y) \sinh[k_n(z - h_1)]$, where $k_n = n\pi/a$, $A_n = -\sum_{m=1}^{\infty} B_m b_m g_{mn} / \sinh(k_n h_1)$, $b_m = \coth(c_m h_2) + c_m \rho_c / \rho_2$, $c_m = (m - 1/2)\pi/b$, $g_{mn} = 2 \int_0^1 dx \cos(n\pi x) \cos(c_m a x)$, and B_n is solved from equation (2) of [7]. Our exact field solution is verified in various known limits [8, 9]. From the exact field solution, we calculate the current density distribution, current flow patterns, as well as contact resistance, which consists of interface resistance and the constriction (spreading) resistance due to current crowding effects.

3. Results

Once the potential $\Phi(y, z)$ inside the region ABCDEFA in figure 1 is obtained from the exact field solution, the current density distribution can be calculated from,

$$J(y, z) = \sigma \sqrt{E_y^2(y, z) + E_z^2(y, z)} = \frac{|\nabla \Phi|}{\rho}, \quad (1)$$

where $\sigma(\rho)$ and E are the electrical conductivity (resistivity) and electric field, respectively. The current flow line equation,

Table 1. Laplace equation and boundary conditions for the model in figure 1^a.

Inside OBCD:	$\nabla^2 \Phi_{\text{I}} = 0$
Inside AOEF:	$\nabla^2 \Phi_{\text{II}} = 0$
At BC:	$\Phi_{\text{I}} = 0$
At EF:	$\Phi_{\text{II}} = V/2$
At OA, OB, CD:	$\partial\Phi/\partial y = 0$
At ED, AF:	$\partial\Phi_{\text{II}}/\partial z = 0$
Across OD:	$J_z = -(1/\rho_1)\partial\Phi_{\text{I}}/\partial z = -(1/\rho_2)\partial\Phi_{\text{II}}/\partial z;$ $\rho_c J_z = \Phi_{\text{II}}(z = 0^-) - \Phi_{\text{I}}(z = 0^+)$

^a J_z is the normal component of current density crossing the interface OD, and $\Phi_{\text{I}}(y, z)$ and $\Phi_{\text{II}}(y, z)$ are the potentials in the contact region and the conducting layer respectively.

$y = y(z)$, is integrated from the first-order ordinary differential equation,

$$\frac{dy}{dz} = \frac{\sigma E_y}{\sigma E_z} = \frac{\partial\Phi/\partial y}{\partial\Phi/\partial z}. \quad (2)$$

Figures 2(a)–(d) shows the current density distribution and current flow lines, varying the specific contact resistivity ρ_c . As ρ_c decreases, current flows are more crowded towards the constriction corner at the edge of the contact. The high current crowding near the constriction corner induces intense local joule heating there. The maximum current density near the constriction corner increases by orders of magnitude as ρ_c decreases from $5 \times 10^{-7} \Omega \text{ cm}^2$ to 0. Current flow lines with percentage of the total current are also plotted. The current transfer length L_T is defined as the length along the interface over which 63.21% ($=1 - e^{-1}$, to match the definition of transfer length used in TLM [6], $L_{\text{TLM}} = (\rho_c/\rho_{\text{sh}})^{1/2}$) of the total current transfers from the conducting layer into the contact, which is plotted in figure 2(e), and is compared with L_{TLM} . Note that there are many data points for the plot in figure 2(e), not merely the four cases in figures 2(a)–(d). The same is true for the contact resistance in figure 2(f), and for similar plots in figures 3–6. In general, L_T increases as ρ_c increases. The upper limit of L_T is bounded by the contact size a . When $\rho_c > 5 \times 10^{-7} \Omega \text{ cm}^2$, L_T approaches $\sim 0.63a = 0.32 \mu\text{m}$. When $\rho_c < 2 \times 10^{-10} \Omega \text{ cm}^2$, L_T converges to constant value of $\sim 0.63h_2 = 0.032 \mu\text{m}$. This agrees with our previous studies that, in the limit of $\rho_c \rightarrow 0$, the transfer length is on the order of conducting layer thickness h_2 , when $ah_2 > 1$ [8, 10]. It is clear that L_{TLM} is accurate only over a limited range of ρ_c .

The total contact resistance is shown in figure 2(f), which is defined as $R_c^{\text{Total}} = R_T - \rho_{\text{sh}}(L/2)/W$, where R_T is the total resistance from EF to BC (figure 1) calculated from our exact model, the second term is the resistance of the conducting layer from EF to DG, and W denotes the width in the dimension perpendicular to the paper. We further decompose $R_c^{\text{Total}} = R_{\text{interface}} + R_1 + R_s$, where $R_{\text{interface}} = \rho_c/aW$ is the resistance of the interface, $R_1 = \rho_1 h_1/aW$ is the resistance from OD to BC, and R_s represents the spreading resistance (constriction resistance) due to current crowding near the contact region. All dimensions and resistivities are defined in figure 1. For the parameters given in figure 2, R_c^{Total} is dominated by

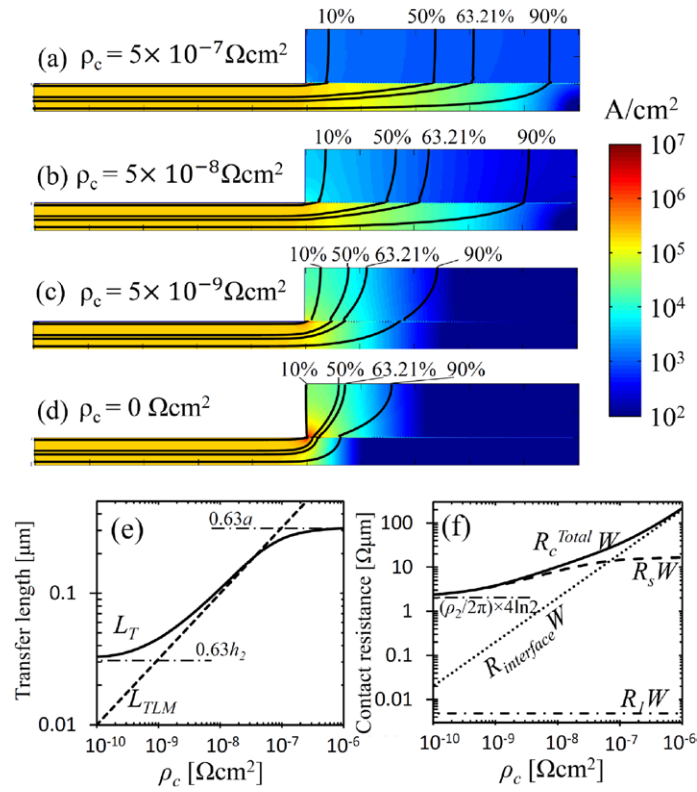


Figure 2. (a)–(d) Current density distribution (color map) and current flow lines (solid lines) calculated analytically from the exact field solution [7]. The percentage near the current flow lines measures the fraction of the total current. (e) Current transfer length L_T and (f) contact resistance $R_c^{Total} = R_{interface} + R_l + R_s$, as a function of interfacial resistivity ρ_c . The transfer length L_{TLM} obtained from TLM is also plotted in (e) for comparison. The parameters used are $a = 0.5 \mu\text{m}$, $L/2 = 10 \mu\text{m}$, $h_1 = 100 \text{nm}$, $h_2 = 50 \text{nm}$, $\rho_1 = 2.44 \times 10^{-8} \Omega \text{m}$, $\rho_{sh} = \rho_2/h_2 = 100 \Omega/\square$. The total current is fixed at $50 \mu\text{A} \mu\text{m}^{-1}$.

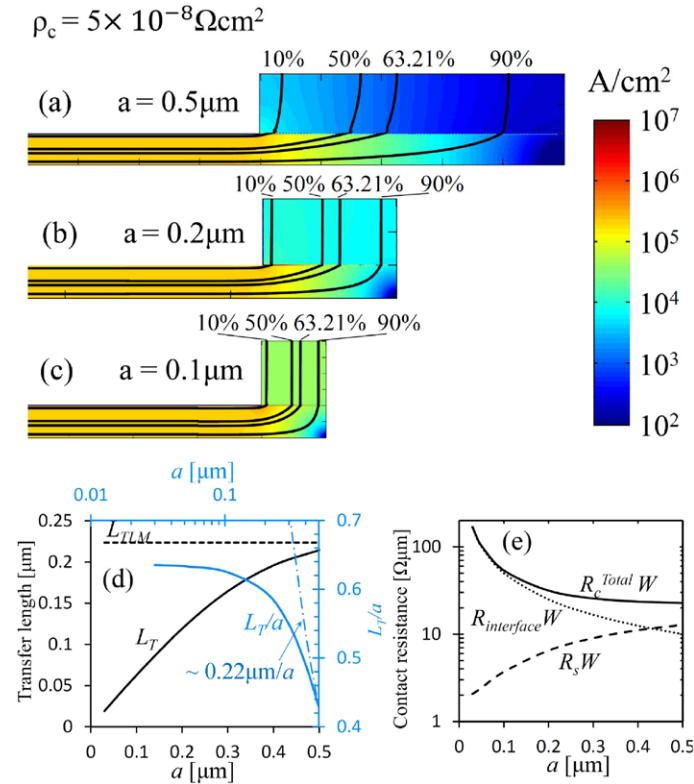


Figure 3. Similar to figure 2 but only a changes. The parameters used are $\rho_c = 5 \times 10^{-8} \Omega \text{cm}^2$, $L/2 = 10 \mu\text{m}$, $h_1 = 100 \text{nm}$, $h_2 = 50 \text{nm}$, $\rho_1 = 2.44 \times 10^{-8} \Omega \text{m}$, $\rho_{sh} = \rho_2/h_2 = 100 \Omega/\square$. As a increases, L_T increases, however L_{TLM} is independent of a . R_c^{Total} decreases with a but converges to $\sim 21 \Omega \mu\text{m}$ for $a > 0.5 \mu\text{m}$, $R_{interface}$ is taken over by R_s when $a > 0.43 \mu\text{m}$. R_l (not shown) is negligible compared to R_c^{Total} .

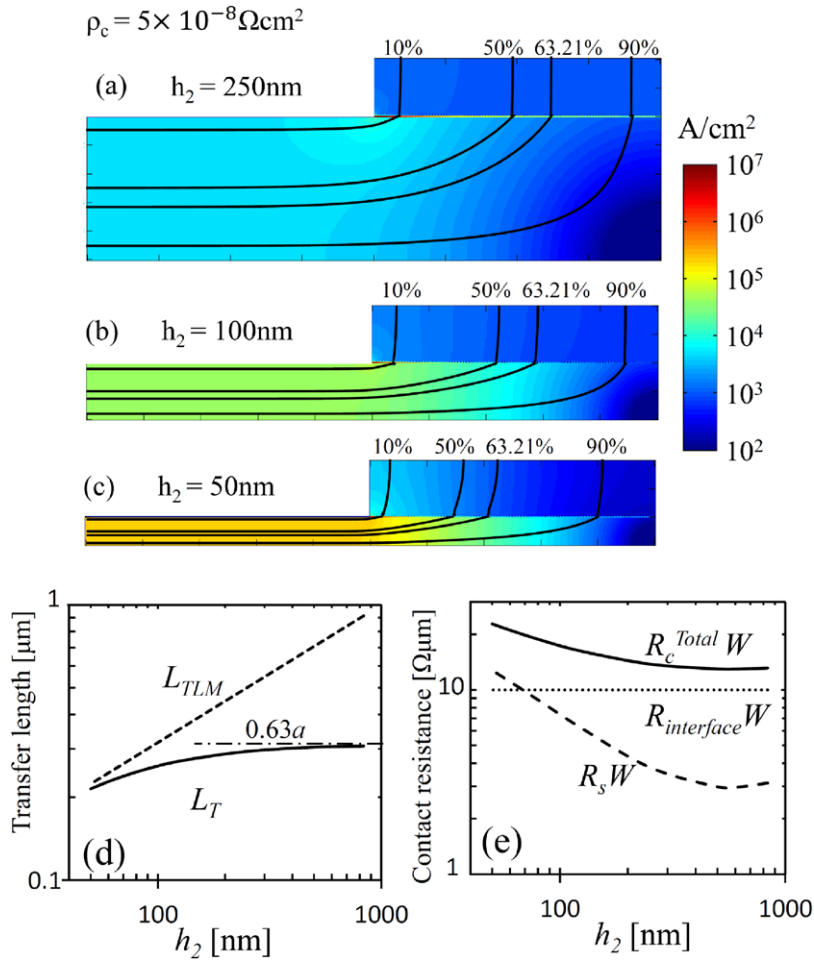


Figure 4. Similar to figure 2 but only h_2 changes. The parameters used are $\rho_c = 5 \times 10^{-8} \Omega \text{cm}^2$, $a = 0.5 \mu\text{m}$, $L/2 = 10 \mu\text{m}$, $h_1 = 100 \text{nm}$, $\rho_1 = 2.44 \times 10^{-8} \Omega \text{m}$, $\rho_{sh} = \rho_2/h_2 = 100 \Omega/\square$. L_T increases with h_2 , but converges to $\sim 0.3 \mu\text{m}$ when $h_2 > a = 0.5 \mu\text{m}$. $R_{interface}$ is independent of h_2 . R_s decreases as h_2 increases when $h_2 < a = 0.5 \mu\text{m}$, but increases with h_2 when $h_2 > a$. Minimum R_s , therefore minimum R_c^{Total} , is achieved when $h_2 = a = 0.5 \mu\text{m}$. R_1 (not shown) is negligible compared to R_c^{Total} .

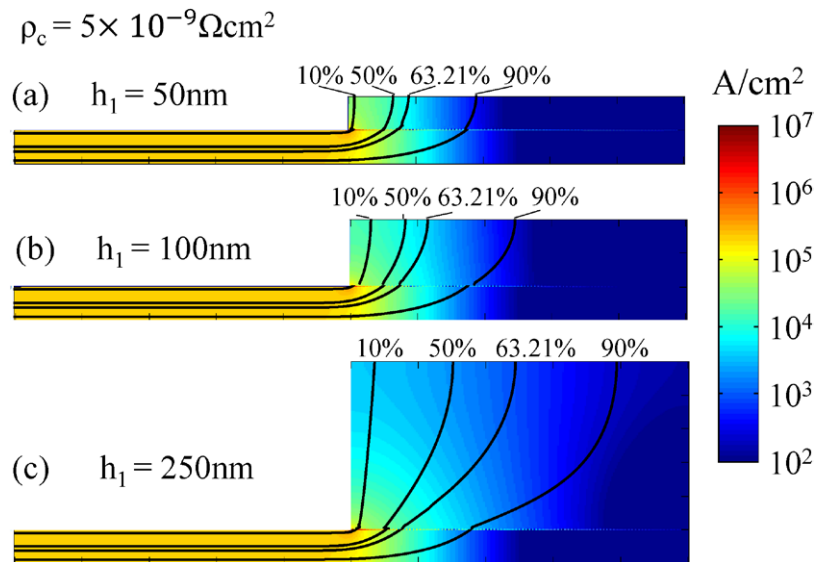


Figure 5. Similar to figure 2 but only h_1 changes. The parameters used are $\rho_c = 5 \times 10^{-9} \Omega \text{cm}^2$, $a = 0.5 \mu\text{m}$, $L/2 = 10 \mu\text{m}$, $h_2 = 50 \text{nm}$, $\rho_1 = 2.44 \times 10^{-8} \Omega \text{m}$, $\rho_{sh} = \rho_2/h_2 = 100 \Omega/\square$. Note that $L_T = 72.5 \text{nm}$, $WR_c^{Total} = 7.4 \Omega \mu\text{m}$, $WR_{interface} = 1 \Omega \mu\text{m}$, and $WR_s = 6.4 \Omega \mu\text{m}$ (not shown) are all independent of h_1 as ρ_1 is highly conductive compared to ρ_2 and ρ_c . However, current spreads to a larger area in the contact region as h_1 increases.

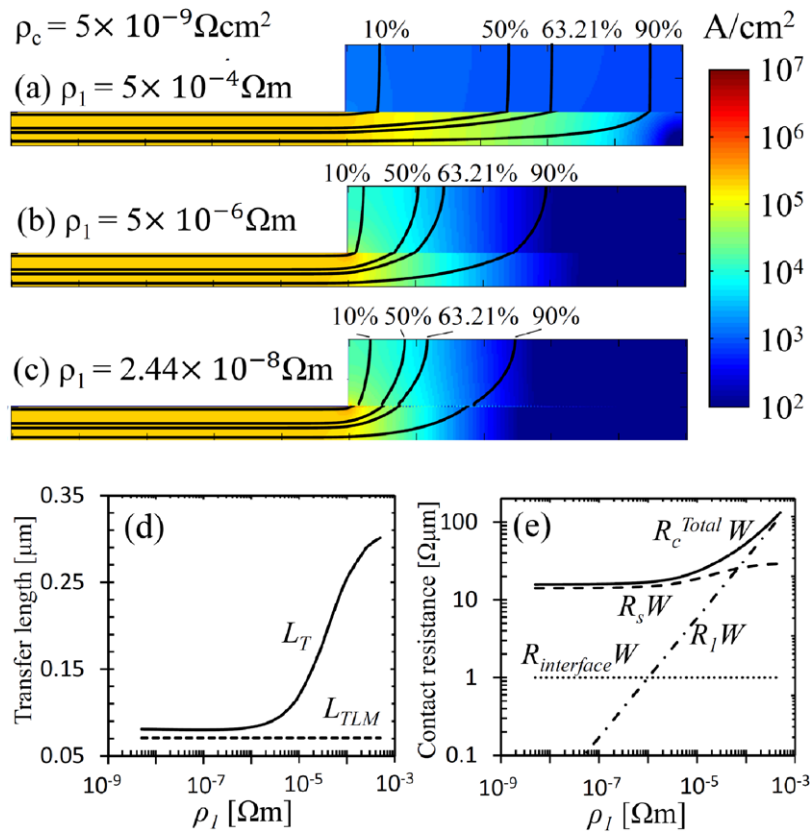


Figure 6. Similar to figure 2 but only ρ_1 changes. The parameters used are $\rho_c = 5 \times 10^{-9} \Omega \text{cm}^2$, $a = 0.5 \mu\text{m}$, $L/2 = 10 \mu\text{m}$, $h_1 = 100 \text{nm}$, $h_2 = 50 \text{nm}$, $\rho_{\text{sh}} = \rho_2/h_2 = 100 \Omega/\square$. L_T is almost constant when $\rho_1 < 10^{-6} \Omega \text{m}$. When $\rho_1 > 10^{-6} \Omega \text{m}$, L_T increases with ρ_1 , where $\rho_1 = 10^{-6} \Omega \text{m}$ corresponds to $R_{\text{interface}} = R_1$, as shown in (e). $R_{\text{interface}}$ is independent of ρ_1 . R_s increases slightly with ρ_1 , whereas R_1 increases linearly with ρ_1 . When $\rho_1 = 10^{-4} \Omega \text{m}$, the contribution of R_1 to R_c^{Total} becomes larger than that of R_s and $R_{\text{interface}}$.

$R_{\text{interface}}$ when $\rho_c > 10^{-7} \Omega \text{cm}^2$, and is dominated by R_s otherwise. When $\rho_c < 2 \times 10^{-10} \Omega \text{cm}^2$, the constriction resistance R_sW , and therefore the total contact resistance R_c^{Total} , converge to constant value of $(\rho_2/2\pi) \times 4\ln 2 = (\rho_2/2\pi) \times 2.77 = 2.2 \Omega \mu\text{m}$. This is the known limit of R_sW derived for $\rho_c \rightarrow 0$ and $ah_2 \gg 1$ [8, 10].

Figure 3 shows that, as the contact size a increases, the current transfer length L_T increases. The transfer length from TLM, $L_{TLM} = 0.22 \mu\text{m}$, is independent of a . L_{TLM} provides an upper limit to L_T , which changes little as the contact size a increases beyond $2L_{TLM}$. The normalized transfer length L_T/a is also plotted as a function of a in figure 3(d). When $a < 0.05 \mu\text{m}$ ($=h_2$), L_T/a is almost a constant $\sim 63\%$. This indicates that when $ah_2 \leq 1$, the relative position of the transfer length (in terms of a) is insensitive to the contact size. When $a > 0.4 \mu\text{m}$, L_T/a scales as $\sim 0.22 \mu\text{m}/a$. This confirms that the actual position of L_T is insensitive to the contact size when $a/L_{TLM} > 2$. As a increases, $R_{\text{interface}}$ decreases because of larger contact area, but the spreading resistance R_s increases. R_c^{Total} decreases with a but converges to constant $\sim 21 \Omega \mu\text{m}$ for $a > 0.5 \mu\text{m}$, which may be estimated from $R_cW = \sqrt{\rho_c\rho_{\text{sh}} + 0.19\rho_{\text{sh}}^2h_2^2}$, for $a \gg h_2$, as derived by Berger [7, 9].

Figure 4 shows that current crowding becomes worse when the thickness of the conducting layer h_2 decreases. When h_2 is small ($< 60 \text{nm} \ll a$), L_T follows closely L_{TLM} , since the TLM approach is expected to be reliable when the thin film thickness

$h_2 \rightarrow 0$ [9]. L_T increases with h_2 , but converges to a constant value $\sim 0.63a = 0.3 \mu\text{m}$ when $h_2 > a = 0.5 \mu\text{m}$. This indicates that, when $h_2/a > 1$, L_T is mainly determined by the contact size a , since the fringing field (therefore the current crowding region) is determined by the smaller dimension near the constriction corner [11]. The resistance due to the interface layer $R_{\text{interface}}$ is independent of h_2 . The spreading resistance R_s decreases as h_2 increases when $h_2 < a = 0.5 \mu\text{m}$, but increases with h_2 when $h_2 > a$. The minimum R_s , therefore minimum R_c^{Total} , is achieved when $h_2 = a = 0.5 \mu\text{m}$, which is consistent with the condition for minimum contact resistance identified previously [8].

Figure 5 shows that the current spreads to a larger area in the contact region as the thickness of the contact region h_1 increases. However, the current transfer length $L_T = 72.5 \text{nm}$ across the contact interface, the total contact resistance $R_c^{\text{Total}}W = 7.4 \Omega \mu\text{m}$, interface resistance $WR_{\text{interface}} = 1 \Omega \mu\text{m}$, and the spreading resistance $WR_s = 6.4 \Omega \mu\text{m}$, are all independent of h_1 , as ρ_1 is highly conductive compared to ρ_2 and ρ_c for the given parameters.

Figure 6 shows that current flows become more crowded near the constriction corner when the resistivity of the contact region ρ_1 decreases. The transfer length L_T is almost constant when $\rho_1 < 10^{-6} \Omega \text{m}$. When $\rho_1 > 10^{-6} \Omega \text{m}$, L_T increases with ρ_1 , where $\rho_1 = 10^{-6} \Omega \text{m}$ corresponds to $R_{\text{interface}} = R_1$, as shown in figure 6(e). The spreading resistance R_s increases slightly with ρ_1 , whereas the resistance of the contact region R_1 increases linearly with ρ_1 . When $\rho_1 = 10^{-4} \Omega \text{m}$, the contribution of R_1 to

R_c^{Total} becomes larger than that of R_s and $R_{\text{interface}}$. Note that it is not possible to obtain the effects of contact electrode properties, ρ_1 and h_1 , on the contact resistance and current transfer length shown in figures 5 and 6 from the TLM approach, which lumps the contact electrode and the resistive interface together.

4. Conclusion

In this paper, current crowding and contact resistance are analyzed by the exact field solution for a contact model, over a large parameter space in resistivity and dimensions of the contact. The current transfer length L_T is compared with that of the transmission line model, L_{TLM} . This paper exemplifies the wide utility of the exact field solution [7] constructed for figure 1. It is found that current crowding effect becomes more severe as the interface specific contact resistivity decreases, the resistivity ratio between the contact and thin film decreases, or the thickness of either contact member decreases. It is found that, if the interface specific contact resistivity ρ_c is small, L_T is bounded by the smaller of the two dimensions—thin film thickness and contact size. As ρ_c increases, L_T increases, but saturates at a constant determined by the smaller of the two dimensions—contact size and L_{TLM} . The total contact resistance is decomposed into three components: the interface resistance due to ρ_c , the spreading resistance due to current crowding, and the resistance due to the contact electrode. The contribution from the individual components of the contacts are examined and compared in detail.

Acknowledgment

This work was supported by AFOSR Grant No. FA9550-14-1-0309.

References

- [1] McNealy B E, Jiang J, and Hertz J L 2015 A precise, reduced-parameter model of thin film electrolyte impedance *J. Electrochem. Soc.* **162** F537–46
- [2] Shane J, Gu Q, Potterton A and Fainman Y 2015 Effect of undercut etch on performance and fabrication robustness of metal-clad semiconductor nanolasers *IEEE J. Quantum Electron.* **51** 2000109
- [3] Grosse K L, Bae M, Lian F, Pop E and King W P 2011 Nanoscale Joule heating, Peltier cooling and current crowding at graphene-metal contacts *Nat. Nanotechnol.* **6** 287
- [4] Nagashio K, Nishimura T, Kita K and Toriumi A 2010 Contact resistivity and current flow path at metal/graphene contact *Appl. Phys. Lett.* **97** 143514
- [5] Yeh E C and Tu K N 2000 Numerical simulation of current crowding phenomena and their effects on electromigration in very large scale integration interconnects *J. Appl. Phys.* **88** 5680
- [6] Schroder D K 1998 *Semiconductor Material and Device Characterization* 2nd edn (New York: Wiley)
- [7] Zhang P and Lau Y Y 2014 An exact field solution of contact resistance and comparison with the transmission line model *Appl. Phys. Lett.* **104** 204102
- [8] Zhang P, Hung D and Lau Y Y 2013 Current flow in a 3-terminal thin film contact with dissimilar materials and general geometric aspect ratios *J. Phys. D: Appl. Phys.* **46** 065502
Zhang P, Hung D and Lau Y Y 2013 *J. Phys. D: Appl. Phys.* **46** 209501 (corrigendum)
- [9] Berger H H 1972 Models for contacts to planar devices *Solid State Electron* **15** 145–58
- [10] Zhang P, Lau Y Y and Timsit R S 2012 On the spreading resistance of thin-film contacts *IEEE Trans. Electron Devices* **59** 1936
- [11] Zhang P 2012 Effects of surface roughness on electrical contact, RF heating and field enhancement *PhD Thesis* The University of Michigan, Ann Arbor